Electronic Supplementary Material

Hybrid Nanomaterial-Based Indirect Electrochemical Sensing of Glyphosate in Surface Water: A Promising Approach for Environmental Monitoring

Elisabeta-Irina GEANĂ[a], Angela Mihaela BARACU[b], Marius C. STOIAN[b], Oana BRÎNCOVEANU[b], Cristina PACHIU[b], Livia Alexandra DINU[b*]

[a]National Institute for Research and Development for Isotopic and Cryogenic Technologies, 4th Uzinei Street 240002, Râmnicu-Vâlcea, Romania

[b]National Institute for Research and Development in Microtechnologies (IMT Bucharest), 126A Erou Iancu Nicolae Street, 077190 Voluntari (Ilfov), Romania

*Corresponding author: livia.dinu@imt.ro

Materials and reagents

Potassium ferrocyanide ($K_4[Fe(CN)_6]$), potassium chloride (KCl), dimethylformamide (DMF), glyphosate (GLY), chlorpyrifos (CHL), glufosinate-ammonium (GLU) and phosmet (PHO) were purchased from Sigma Aldrich (Germany). $K_4[Fe(CN)_6]$ was used as redox probe and the 1mM stock solution was prepared by dissolving 11.9 mg in 25 mL of 0.2M KCl, as supporting electrolyte. GLY was dissolved in water to obtain a stock solution of 1000 ppm. For lower concentrations of GLY, the serial dilution method was used, the final GLY solution containing also Britton-Robinson buffer (BRB) of optimum pH and 0.1M KCl, as supporting electrolyte. All the other solutions of herbicides were prepared similar to the GLY solution.

The electrochemical transducer was a screen-printed carbon electrode from Metrohm (product code: DRP-110) consisting in a three-electrode system. The working (WE) and auxiliary electrodes (CE) were patterned using a carbon ink dispersion, while the reference electrode (RE) was printed using a silver ink. The substrate was a ceramic isolating layer with dimensions of 3.4 × 1.0 × 0.05 cm (length × width × thickness)

*Apparatus and method*s

All electrochemical and impedimetric measurements were performed with an AUTOLAB/PGSTAT 302N (Metrohm) connected to a personal computer. For the electrochemical characterization, cyclic voltammetry (CV) and electrochemical impedance spectroscopy (EIS) were used. The EIS data were fitted with the appropriate equivalent electrical circuits, using NOVA Fit. Typical CVs of the redox process were recorded in the potential range from −0.40 to 0.60 V, at 20mV/s scan rate.

Scanning electron microscope (SEM) and Energy Dispersive Spectroscopy (EDAX) were used to characterize the surface morphology and composition of the Au-GR nanohybrid material. The surface morphology of the Au-GR nanohybrid samples were acquired with a Nova

NanoSEM 630 Scanning Electron Microscope (FEI Company, Hillsboro, OR, USA) using UHR detector (Through-Lens-Detector-TLD) at an acceleration voltage of 15 kV.

Raman spectroscopy measurements were achieved with a Witec Alpha 300S/2008 Gmbh Germany system equipped with a 532 nm laser in backscattering configuration by 600 grooves/mm grating and 10 s acquisition time. We used a Thorlabs100x microscope with a laser spot size of about 400 nm and 1mW power, and the spectral resolution was calculated at ~ 2 cm^{-1}.

X-ray diffraction (XRD) pattern was acquired with Rigaku SmartLab diffraction system, equipped with a CuKα1 radiation (λ = 1.5406 Å), operated at 45 kV and 150 mA, with 2θ from 5° to 90°.

Fourier-transform infrared (FTIR) spectrum was acquired using the VERTEX 80/80v FT-IR spectrometer, from Bruker Optics, equipped with reflectivity module, at an incidence angle of 50 degrees, in the 4000 – 400 cm^{-1} spectral domain with a resolution of 4 cm^{-1}.

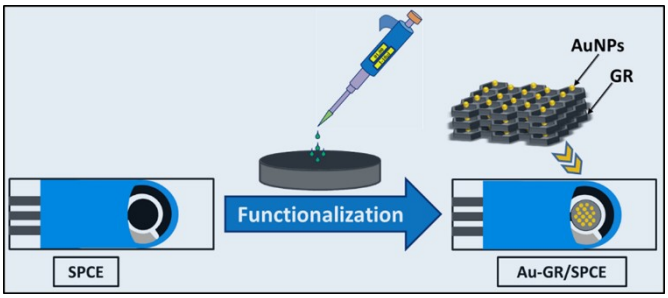

Figure A1. The functionalization protocol of the SPCE using the nanohybrid material Au-GR dispersion

XRD characterization

The gold nanoparticles decorated graphene sensor was analyzed by X-ray diffraction and the XRD pattern is shown in Figure A2a, with the characteristic peaks of the components from the hybrid material. The presence of the gold nanoparticles in the sensor is evidenced by the diffraction peaks found in the XRD pattern at 2θ = 38.1°, 44.2°, 64.4°, and 77.4°, which can be attributed to (111), (200), (220), and (311) crystalline planes. At the same time, a major

sharp diffraction peak from the carbonic material can be seen at 2θ = 26.5°, corresponding to a multi-layer graphene phase (MLG), similar to a graphite-like material, alongside other minor peaks at 2θ = 35.1°, 43.2°, 52.5°, and 57.4°, arising from the graphite rod precursor used in the preparation method of the hybrid material [1–3].

The average crystallite size of the components was calculated using the Scherrer equation:

$$D = \frac{K\lambda}{\beta cos\theta} \quad (1)$$

where D is the mean crystallite size, K is the shape factor, taken as 0.93, λ is the Cu $K_{\alpha 1}$ X-ray wavelength (λ = 0.15406 nm), θ is the Bragg diffraction angle and β is the full width at half maximum (FWHM) of the diffraction line, in radians.

The crystallite size for the gold nanoparticles was found to be around 35.3 nm, whereas for the graphene material, its crystallite size was evaluated at around 26 nm. For calculating the inter-layer distance between the graphene layers in MLG phase, it was applied the Bragg's law ($n\lambda = 2d\sin\theta$, where n is the diffraction order, λ is the wavelength of the radiation, d is the inter-layer distance, and θ is the incidence angle), in order to obtain an interplanar spacing of ~ 0.336 nm. According to the crystallite size and its interplanar spacing [1], the MLG phase contains an average of 77 layers in the graphene material, wherein gold nanoparticles can be accommodated for better conductivity and improved electrochemical properties.

Raman characterization of Au-GR

Raman spectroscopy is one of the most widely used technique to characterize the defects, doping and strains in the carbonic materials. The evolution of the Raman spectrum depends on the disorders induced in the material structure and this is reflected in the defect-activated Raman intensities.

In the Raman spectrum of GR (A2b), three prominent modes were highlighted: at ~1337.8 cm^{-1} (D band - lattice defects of E_{1g} mode are disordered sp^3 bonded C and it only appears in the presence of defects); at ~1563.4 cm^{-1}(G band - E_{2g} mode is the correspondent to in-plane stretching of ordered sp^2 bonded C) and at ~2672.1 cm^{-1} (2D band - is the secondary D mode with the largest intensity in single layer GR, but it is broadening and reducing in intensity in multi-layer GR; observed even without any disorder or defects). For these modes, the intensity will be denoted as I(D), I(G) and I(2D) respectively, the most important values in characterizing

the GR-like quality of a film. The I_{2D}/I_G ratio makes possible to determine the number of GR layers : when the I_{2D}/I_G ratio is ~ 0.5 as it is in our case, the graphene film has more than 4 layers [4]. This parameter is not relevant when the carbon materials are doped or have impurities as it is the case for the sample Au-GR. The ratio I_D/I_G is an important parameter in the Tuinstra - Koenig relation [5] used to calculate the crystallite size simultaneously with the number and/or the size of sp^2 cluster in the GR material. For small defect concentrations in Au-GR, I(D) is practically constant, while I(G) and I(2D) strongly increase with the concentration of the nanohybrid material Au-GR. A decrease in I_D/I_G ratio (0.56 for GR sample and 0.41 for Au/GR) can be assigned to a decrease in the number and/or the size of sp^2 clusters.

FTIR characterization

FTIR spectra of the Au-GR sensor revealed the vibration modes of hybrid material based on graphene, which were assigned as follows (Figure A2c): a broad band at 3576 cm^{-1} for –OH stretching, 2968 and 2868 cm^{-1} for the asymmetric and symmetric stretching of $–CH_2$, 1614, 1514 and 1463, corresponding to the C=C aromatic stretching vibrations, 1374 cm^{-1} for C-H deformation vibration, 995 and 811 cm^{-1} attributed to C=C–H deformations, 627 and 488 cm^{-1} can be ascribed to the bending and out-of-plane vibrations of the C–H bonds [6].

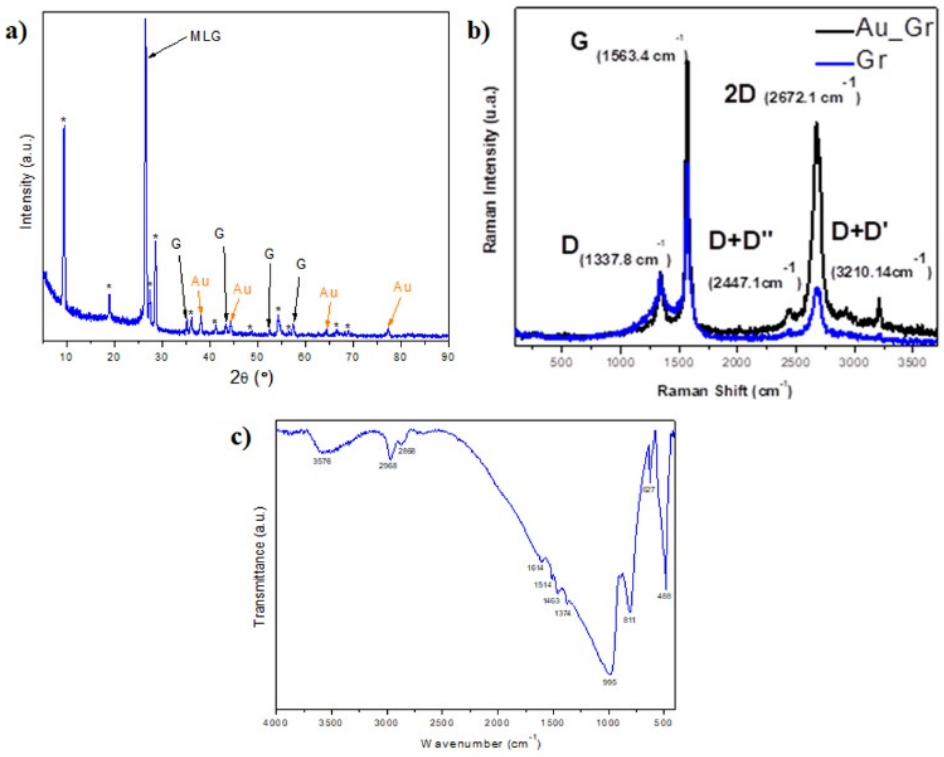

Figure A2. a) The XRD pattern of the Au-Gr sensor, showing characteristics peaks of gold and graphene material (* - substrate, MLG – multi-layer graphene, G – graphite); b) Raman spectra on GR (blue line) and Au-GR (black line); c) FTIR spectrum of the Au-GR sensor with the vibration

modes of the hybrid material.

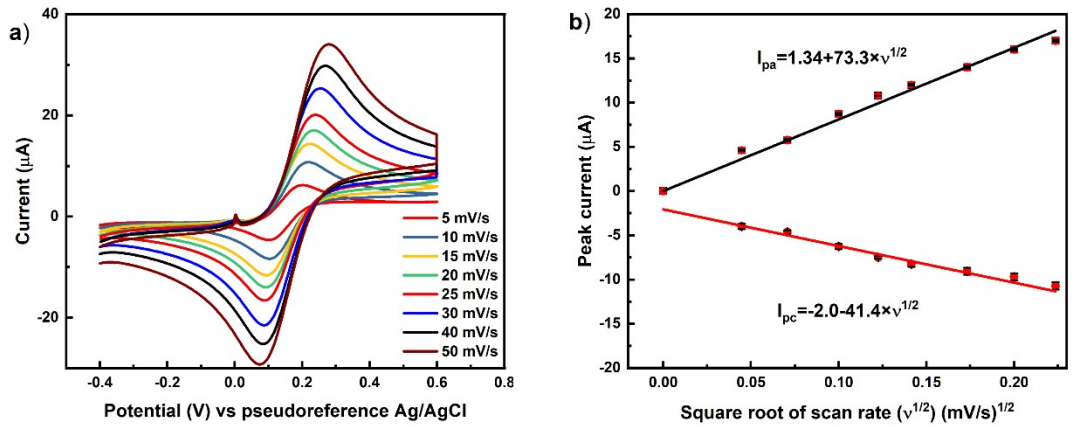

Figure A3. a) CVs of SPCE recorded in 0.2M KCl containing 1 mM $K_4[Fe(CN)_6]$ at different scan rates; b) anodic and cathodic peak current versus square root of scan rate ($\nu^{1/2}$)

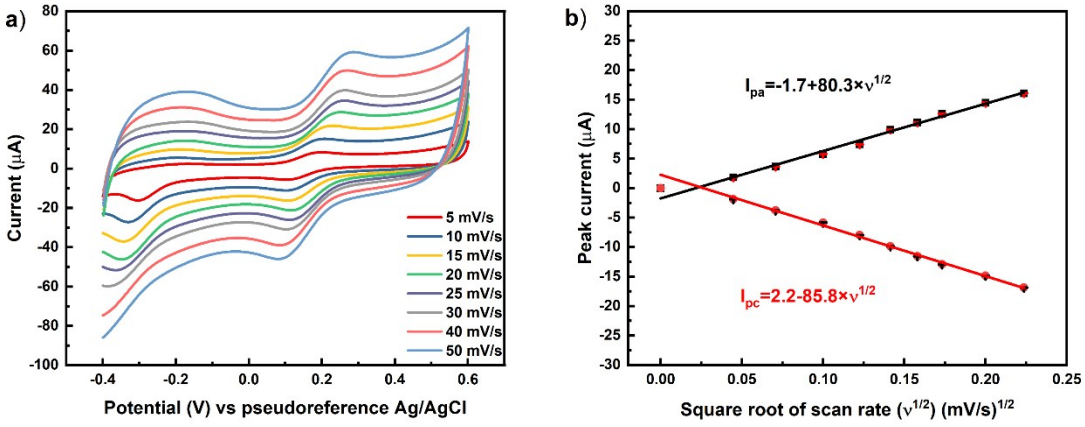

Figure A4. a) CVs of GR/SPCE recorded in 0.2M KCl containing 1 mM $K_4[Fe(CN)_6]$ at different scan rates; b) anodic and cathodic peak current versus square root of scan rate ($\nu^{1/2}$)

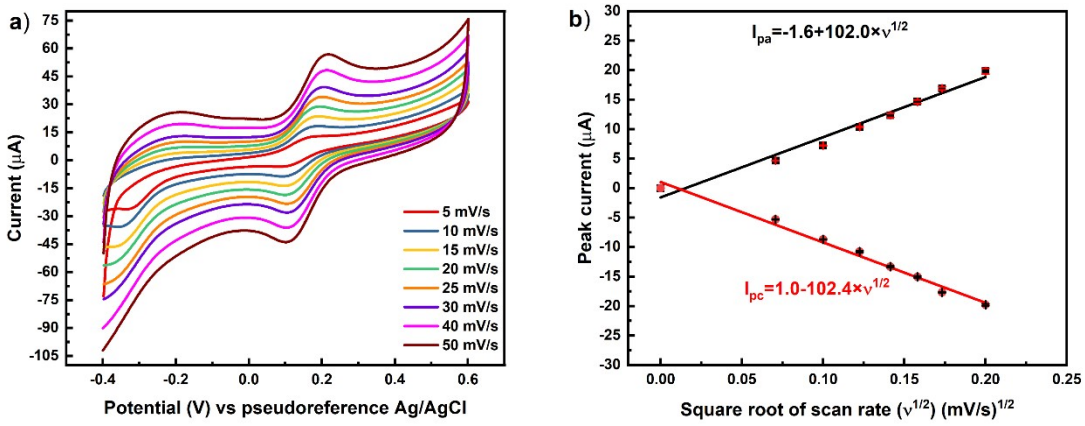

Figure A5. a) CVs of Au-GR/SPCE recorded in 0.2M KCl containing 1 mM $K_4[Fe(CN)_6]$ with the Au-GR/SPCE at different scan rates; b) anodic and cathodic peak current versus square root of scan

rate ($\nu^{1/2}$)

Table A1. Electrochemical parameters of the tested SPCEs.

Sensor	Active area (A) (cm^2)	Δ Ep (mV)	Rct (Ω)	K_{app} (cm/s)
SPCE	0.109	120	3240	7.54×10^{-4}
Gr/SPCE	0.113	110	168	1.40×10^{-2}
Au-Gr/SPCE	0.157	85	48	3.53×10^{-2}

Table A2. Analytical parameters of the Au-Gr/SPCE measured in buffer and surface water matrix.

	Buffer	Surface Water
Linear range (ppb)	0.1 - 10 10 - 100	0.1 - 80
Slope (µA/ppb)	-2.09 -0.11	0.30
Standard error of the slope	±0.1 ±0.03	±0.05
Intercept (µA)	-66.0 -46.4	-24.8
Correlation coefficient	0.9996 0.9975	0.9995
LOD (ppb)	0.03	0.03
LOQ (ppb)	0.1	0.1

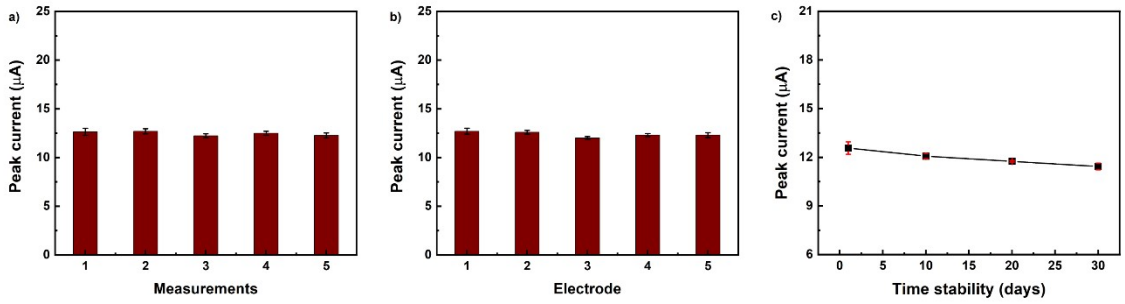

Figure A6. (a) Repeatability (b) reproducibility, and (c) time stability of Au-GR/SPCE

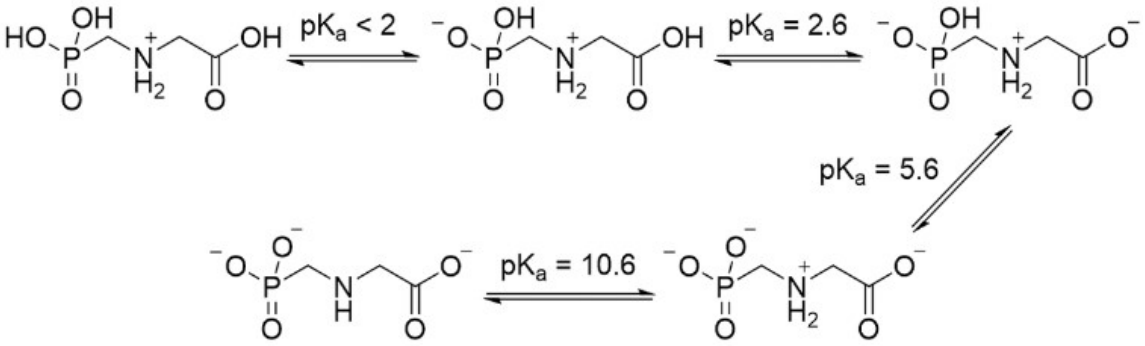

Figure A7. Dissociation constants and the corresponding ionic structures of GLY

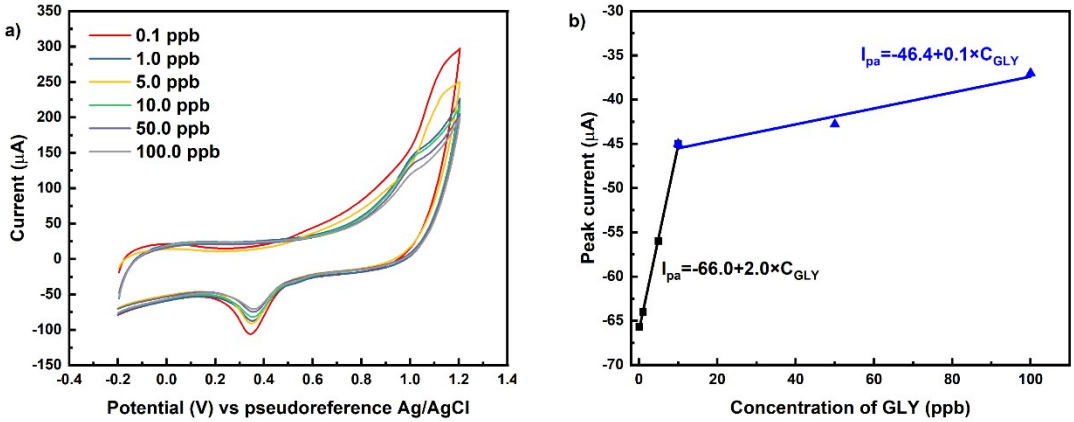

Figure A8. a) Measurements recorded using the developed sensor based on Au-GR/SPCE for pH 5 BRB containing six different GLY concentrations in a range from 0.1 ppb to 100 ppb and b) the peak current (Ipa) plotted vs the concentration of GLY

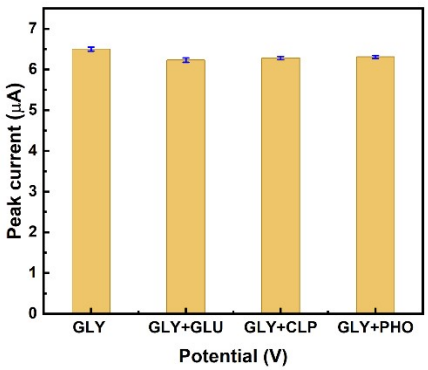

Figure A9. Response of the Au-Gr based sensor in pH 5 BRB buffer containing 10 ppb GLY without and with other possible interfering species: glufosinate ammonium (GLU), chlorpyrifos (CLP) and phosmet (PHO).

References

1, Livia Alexandra Dinu Gugoasa, Florina Pogacean, Sevinc Kurbanoglu, Lucian Barbu-Tudoran, Andreea Bianca Serban, Irina Kacso and Stela Maria Pruneanu, Graphene-Gold Nanoparticles Nanozyme-Based Electrochemical Sensor with Enhanced Laccase-Like Activity for Determination of Phenolic Substrates, *J. Electrochem. Soc.*, 2021, **168**, 067523.

2, R. Siburian, D. R. Sari, J. Gultom, H. Sihotang, S. L. Raja, J. Gultom and M. Supeno, Performance of graphite and graphene as electrodes in primary cell battery, *J. Phys. Conf. Ser.*, 2018, **1116**, 042034.

3, S. Gea, J. N. Sari, R. Bulan, A. Piliang, S. A. Amaturrahim and Y. A. Hutapea, Chitosan/graphene oxide biocomposite film from pencil rod, *J. Phys. Conf. Ser.*, 2018, **970**, 012006.

4, Andrea C. Ferrari, Raman spectroscopy of graphene and graphite: Disorder, electron–phonon coupling, doping and nonadiabatic effects, *Solid State Commun.*, 2007, **143**, 47–57.

5, F. Tuinstra and J. L. Koeing, Raman Spectrum of Graphite, *J. Chem. Phys.*, 1970, **53**, 1126.

6, G. Socrates, Infrared and Raman characteristic group frequencies. Tables and charts, in *Journal of Raman Spectroscopy*, 2001, p. 347.